Full-waveform inversion for imaging and geologic interpretation: A deepwater Gulf of Mexico case study

Yannick Cobo[1], Carlos Calderón-Macías[1], and Shihong Chi[1]

Abstract

Full-waveform inversion (FWI) is commonly used in model-building workflows to improve the resolution of the shallow velocity model and thus has a potentially positive impact on the imaging of deeper targets. This type of inversion commonly makes use of first arrivals from the longest offsets. However, signal from smaller offsets and later times can extend the depth range of the FWI-derived velocity model. Waveform inversion methods that use reflections have been shown to provide greater details and accuracy when deriving velocity models for deepwater exploration and production. The derived velocity sometimes provides an improved migrated image useful for interpretation in complex geology and enhances geologic features such as subsalt sediments, faults, and channels. We have used combination of FWI and a wavefield inversion approach known as reconstructed wavefield inversion (RWI) that makes use of diving waves and reflections to derive a velocity model for a deepwater survey off the coast of Veracruz in the Gulf of Mexico. The velocity model we derived from this approach produces an improved image of the target reservoir, and furthermore contains enough geologic details for direct interpretation. We enhanced the resolution of the velocity model further by performing a poststack amplitude inversion with the FWI + RWI derived velocity used as the input low-frequency model. The resulting high-resolution velocity provides an excellent product for detecting shallow gas anomalies, delineating a gas reservoir in an anticline structure as well as a system of deep, sand-filled channels. The inverted velocity also indicates a better correlation with sonic velocity measured from two blind wells than the initial tomography velocity, indicating the benefits of FWI approaches for quantitative reservoir characterization in deepwater environments.

Introduction

One of the most significant trends in seismic imaging of complex geology corresponds to the transition of ray-based methods to wavefield extrapolation methods for imaging and velocity estimation. Reverse time migration (RTM) allows a geophysicist to image steeply dipping and overhanging reflectors that are difficult to resolve with a ray-based method such as Kirchhoff migration. RTM in combination with wide azimuth and long-offset acquisition geometries has produced the highest resolution images in complex geology such as subsalt reservoirs in the deepwater Gulf of Mexico (GOM) (e.g., Huang et al., 2011). More recently, full-waveform inversion (FWI) is being used to provide a more accurate shallow velocity model than is possible by ray-based reflection tomography (Sirgue and Pratt, 2004; Tarantola, 1984; Virieux and Operto, 2009), with best results being obtained when low frequencies and long offsets are recorded (e.g., Chen et al., 2018). For conventional marine streamer acquisition, FWI uses diving waves to update the shallow sediment velocities up to a depth equal to a fraction (typically 1/3 to 1/2) of the maximum offset; this effectively limits the extent of the model update in deepwater scenarios. To increase the depth range in the model estimation process, it has commonly been necessary to use reflections and diving waves through a combination of ray-based tomography and conventional (diving wave) FWI, aided in some cases with interpretation and inclusion of salt bodies in the model. Reflections can also be incorporated into FWI. Recently, this approach has been pursued with some modifications to the conventional one such as the use of a reflectivity model as a prior to generate the reflections (Brossier et al., 2013; Liu et al., 2015), by introducing density into FWI (e.g., Yang et al., 2016; Peng et al., 2018) or an extension of FWI that includes a reconstruction of the source wavefield (Van Leeuwen and Hermann, 2013; Wang et al., 2017). Diving wave energy relies on a continuous increase of velocity with depth, whereas, reflections are caused by sharp impedance contrasts, which can be introduced into the model by the use of a priori information such as

a migrated section to act as reflectivity model or an initial density model that is somehow tied to the reference velocity model and reflectivity. Diving wave FWI and reflection FWI have been used recently for improving the velocity model in deepwater salt scenarios. Shen et al. (2018) demonstrate that, for the Atlantis Field in the deepwater GOM, low frequencies and long offsets acquired with a node acquisition survey enabled FWI to derive velocity models containing salt bodies with little or no additional manual salt body interpretation when starting from a legacy model containing interpreted salt bodies; Vigh et al. (2016) expand the depth range of velocity estimation with data from the same area by incorporating reflections in FWI that results in an improved subsalt image; and Peng et al. (2018) use diving wave FWI and reflections with an FWI method that allows for density contrasts in a wide azimuth data set from the Perdido fold belt in the Western GOM — this also resulted in an improved subsalt velocity model and image. More recent development on these topics can be found in Zhang et al. (2018) and Chen et al. (2018).

In other cases, the wavefield approaches such as RTM and FWI have been used for applications such as amplitude variation with offset and post and prestack inversion studies. Conventional RTM and FWI are based on propagation in an acoustic medium. Although there are recent efforts to extend these methods to the elastic case (Chang and McMechan, 1994; Lu et al., 2013), these approaches are not currently used in industry primarily due to their inherently high computation cost. Despite the acoustic approximation most often used in FWI, inverted high-resolution velocity models can help improve the structural definition of a reservoir and potentially be useful for quantitative interpretation studies as shown, for instance, in the work by Routh et al. (2017), where a 40 Hz acoustic FWI resulted in a high-resolution impedance model that provided a good match with information from wells. In their work, the model derived with FWI was used in conjunction with the conventional seismic volumes for identifying potential shallow drilling hazards.

Quantitative seismic interpretation relies on inversion methods that take advantage of amplitude information in the stack or gathers. Classical quantitative inversion methods require a low-frequency model (LFM) because the migrated seismic data typically lack low-frequency content. An LFM is typically built by extending the well data within a structural framework interpreted from the seismic stack. This well-based technique is often biased due to the limited number of available wells and the limited geologic detail represented in the structural model. Independent seismic velocities may be brought in, to try to reduce the LFM bias by the well information. Significant obstacles still exist for this application due to the difficulties of converging from seismic derived velocities to elastic rock properties (e.g., Sams and Carter, 2017). Due to the very low-frequency content of seismic velocity (often in the range of 0–2 Hz), a frequency gap typically exists between the spectra of seismic velocity and seismic stacks or gathers. High-resolution FWI-derived velocities can potentially close the gap and produce an unbiased
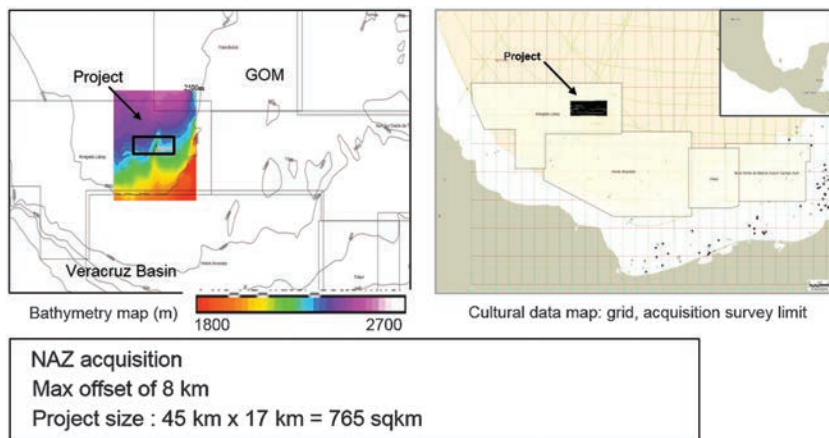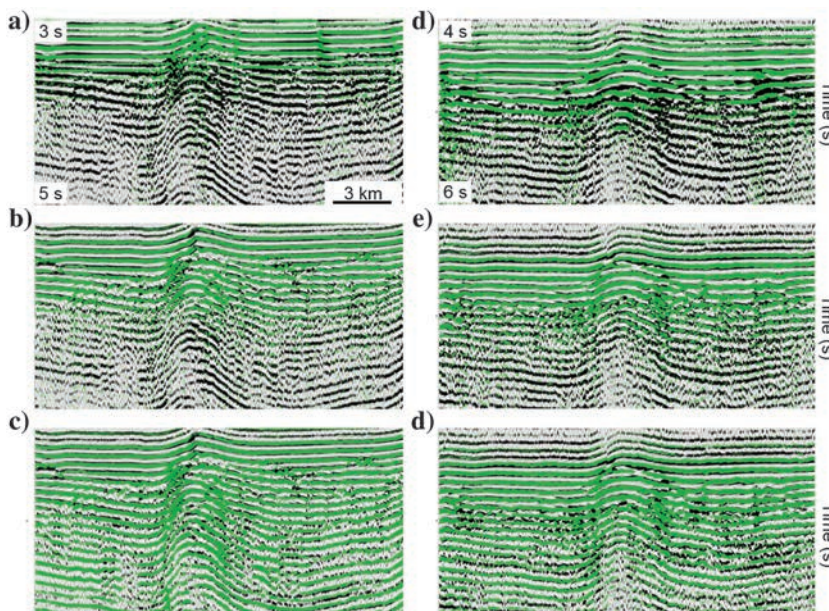

Figure 1. Location map.

Figure 2. Common channel gathers. Modeled data (green) are overlaid on field data (black). (a-c) Near and (d-f) far channels, approximately 1000 and 5000 m offset, respectively, for (a and d) tomography model, (b and e) diving wave FWI, and (c and f) RWI method (data processed by ION in partnership with Schlumberger, who holds the data licensing rights).

direct LFM for amplitude-based inversion for quantitative inversion.

In this work, we derive a velocity model from a narrow azimuth (NAZ) survey in the Mexican side of the GOM using diving waves and reflections. The area under investigation is characterized by folding, gas-bearing sand channels, and faulting. Reflection tomography is able to capture the overall trend of reflectors following an anticline structure, but the velocity model lacks detail for delineating shallow and deep faulting and loses resolution at intermediate depths. We perform FWI in the time domain using primarily the diving wave information at the longer offsets starting from the tomography inverted model. The FWI implementation we use here is acoustic, assumes constant density and anisotropy of the vertically transverse isotropy type (Wang et al., 2014). Using the result model from the previous step as a starting model, we invert for the deeper velocity by making use of the diving waves and reflections with the reconstructed wavefield inversion (RWI) method (Wang et al., 2017). This method extends the cost function to depend on velocity and a reconstructed source wavefield that varies with space and time and that is built from the mismatch obtained from predicting the reflections and refractions in the data. The relative importance of the source reconstruction term depends on an a priori parameter that is particularly useful at the start of the inversion by relaxing the need for closely matching synthetic and predicted data at the selected scale or frequency band being inverted. This approach has the advantage of not being constrained with any additional a priori information or assumptions about density or reflectivity. Both FWI approaches used here rely on the conjugate gradient minimization method to update the velocity model.

A key aspect of the proposed scheme is the top-down approach that first solves for shallow details with the combination of tomography and conventional FWI. We compare the inverted velocities at each stage with available well-log data. We then perform three model-based poststack inversions to invert velocity to take advantage of the amplitude data. The inputs to our post-stack inversion are a stack from the RTM migrated seismic using the final FWI velocity, comprising the tomography and the two waveform inversion steps, and three LFMs, which are (1), the velocity resulting from ray-based

tomography; (2), the velocity obtained by extrapolating the well velocity within the structure framework interpreted from the migrated image; and (3), the final FWI velocity. We first describe the area of investigation and seismic data and follow with a description of the model-building workflow and the results of our inversions.

Description of the area of investigation and data preprocessing

The study area is centered on a gas/wet gas discovery located at approximately 125 km off the cost of Mexico's Veracruz state (Figure 1), and the water depth is approximately 2000 m. This area is of interest due to
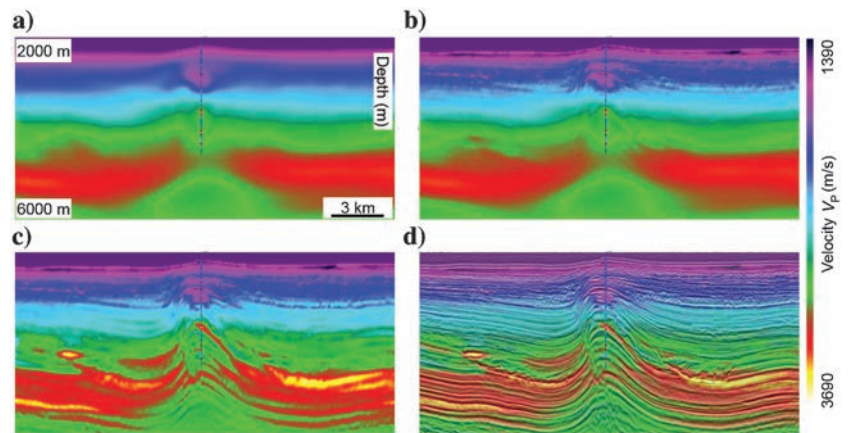
Figure 3. Inline section through well location. P-wave velocity model (a) after ray tomography, (b) diving wave FWI, (c) RWI method, and (d) diving wave FWI and RWI method with corresponding 60 Hz RTM stack. Well-log velocities plotted at center (data processed by ION in partnership with Schlumberger, who holds the data licensing rights).
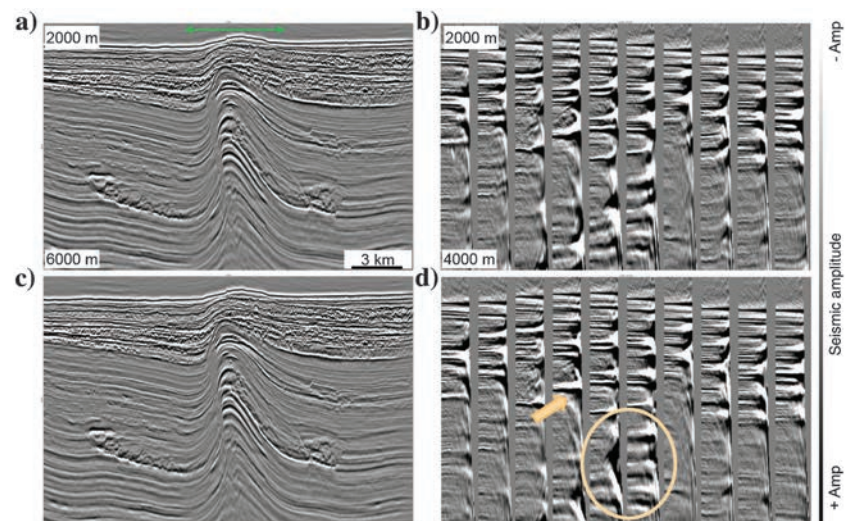
Figure 4. Kirchhoff prestack depth migration and common-image gathers for a different inline than the one displayed in Figure 3 (data processed by ION in partnership with Schlumberger, who holds the data licensing rights). (a and b) Using ray tomography velocity and (c and d) using diving wave FWI and RWI velocity.

the large gas accumulations in structural plays that cause rapid velocity variations. The area is also characterized by folding and faulting, with an anticline structure at the center of the investigation area. There are two wells in the area with velocity information. Their locations are plotted in Figure 1 alongside the bathymetry. Seismic data were acquired with an NAZ survey with a maximum offset of 8.4 km. The lowest frequency with useful signal in the data is approximately 4 Hz. We implemented a standard processing flow that includes basic denoise, debubble, source and receiver deghosting, zero phasing, and multiple removal.

MODEL BUILDING WITH FWI AND RWI

The model-building workflow comprises ray-based reflection tomography followed by waveform inversion of diving and reflected events. The staging of the model-building processing and quality control is summarized by the data and model displays from Figures 2 and 3 for an inline that passes through one of the blind wells in the area of investigation with the well velocity shown in the model displays of Figure 3 with the same color palette used to display the seismic velocities. The left column of Figure 2 shows a common near-channel (approximately 1000 m offset) prestack data section, whereas the right column shows a common far channel (approximately 5000 m offset). The synthetic data are shown in the green color overlying the field data plotted in the black color. The synthetic data are modeled using

a VTI anisotropy acoustic-wave propagator for constant density and an absorbing boundary at the top of the model consistent with the processing of the input data, which is also the modeling engine used by FWI to update the velocity model (Wang et al., 2014). Synthetic data obtained for the reflection tomography velocity model are displayed in Figure 2a and 2d, and the corresponding velocity is shown in Figure 3a. We computed the synthetic data with the anisotropic parameters (delta and epsilon) derived from the available well information. The anisotropic parameters are laterally homogeneous across the model and were not updated during the velocity building process. They are consistent with typical anisotropy used in this area of the GOM. For delta, we used a maximum value of 0.1 throughout the model that is tapered to zero at the water, and epsilon was set to twice that amount. At the reservoir level, delta is close to 0.04 and epsilon is close to 0.08. The resulting velocity model from ray-based tomography generates a relatively smooth model with an area of relatively low velocity toward the middle of the section at a depth of approximately 3000 m. Due to the overall smoothness of the model, the synthetic data mostly contain diving wave events that approximately match the early field data arrivals as noted from Figure 2d.

Starting from the ray-based tomography velocity model, we performed FWI in four frequency bands, from 4 Hz up to a maximum frequency of 10 Hz. The
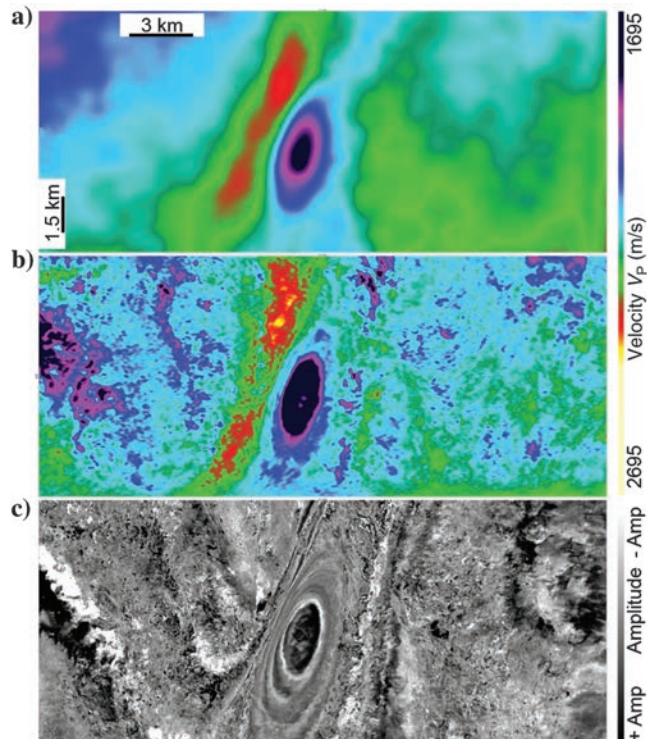
Figure 5. Depth slices at 2860 m from (a) ray tomography velocity model, (b) final FWI velocity model, and (c) 60 Hz RTM stack (data processed by ION in partnership with Schlumberger, who holds the data licensing rights).
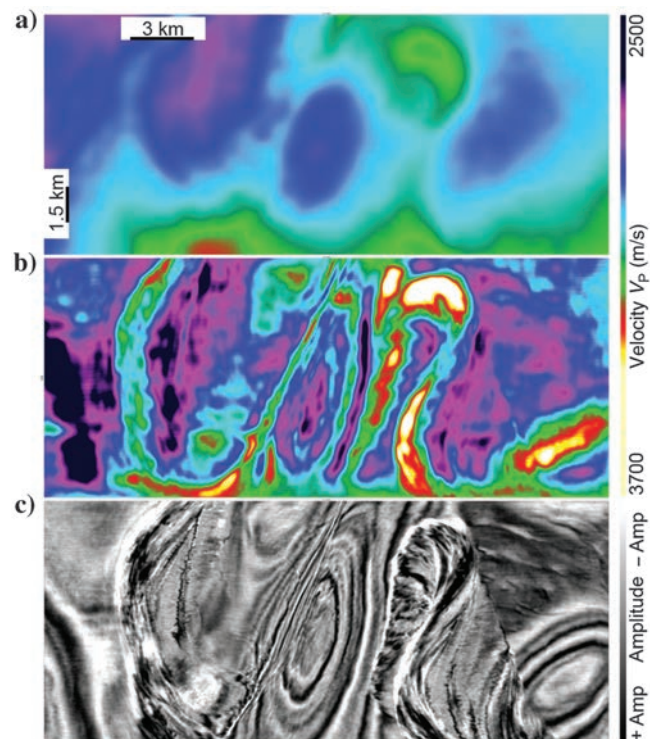
Figure 6. Depth slices at 4620 m from (a) ray tomography velocity model, (b) final FWI velocity model, and (c) 60 Hz RTM stack for final model (data processed by ION in partnership with Schlumberger, who holds the data licensing rights).

synthetic data and the corresponding FWI inverted velocity model are shown in Figures 2b, 2e, and 3b. The FWI method perturbs the reference velocity model to a depth of up to 3400 m corresponding to the depth range that diving waves propagate in the model. The resulting model produces a much clearer definition of the top of the anticline gas-bearing area and resolves shallow low-velocity zones away from the top of the anticline structure. The FWI inverted velocity model produces an improved data fit for the shallow reflections as well as for the longer offset arrivals from the anticline structure observed in Figure 2b and 2e. To increase the vertical and lateral resolution of the velocity model below the maximum depth limit imposed by the maximum available offset and the diving wave FWI method, reflected events need to be incorporated into the inversion. In this work, we use the RWI method as described by Wang et al. (2017). Similar to our FWI results, the propagation assumed for RWI is acoustic with constant density and VTI anisotropy and is also applied in the same frequency bands (from 4 to 10 Hz). The starting model for this inversion is the model after FWI that has been used to update the shallow model. The final FWI + RWI

inverted velocity, described from here on as the final FWI model, is shown in Figure 3c. The final velocity model shows a higher resolution for mapping the structure and delimiting faults and vertical velocity variations not present in the initial tomography velocity model, corroborated by the well velocities overlaying
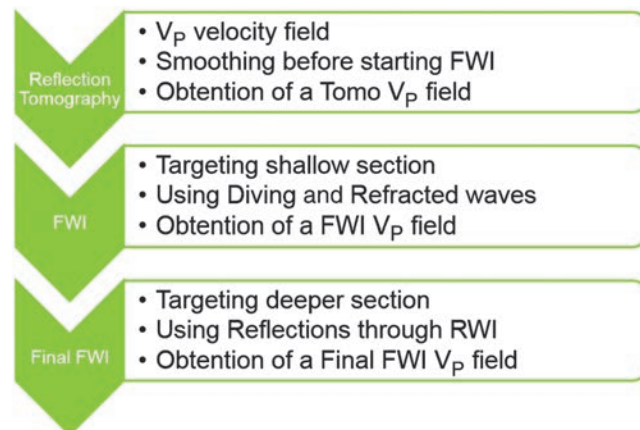

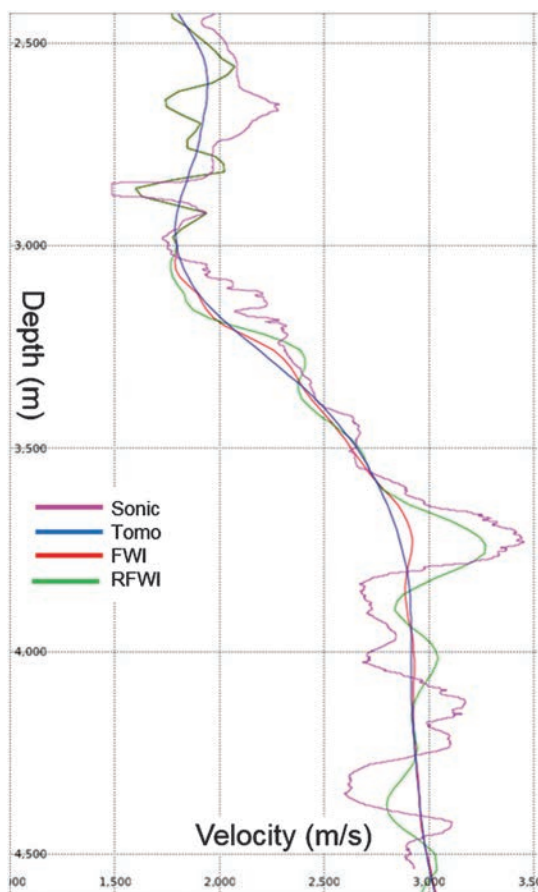**Figure 8.** Flow chart of the model-building process.

Figure 7. Velocity profile at the well location. The purple line is the sonic velocity, the dark blue is the initial ray tomography velocity, the red is the FWI inverted velocity, and the green is the final FWI velocity (data processed by ION in partnership with Schlumberger, who holds the data licensing rights).
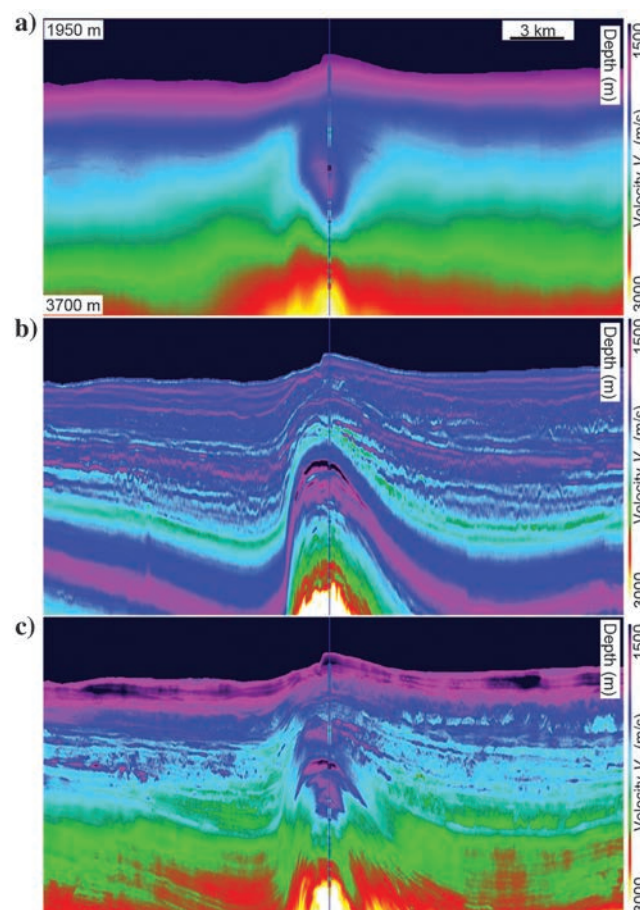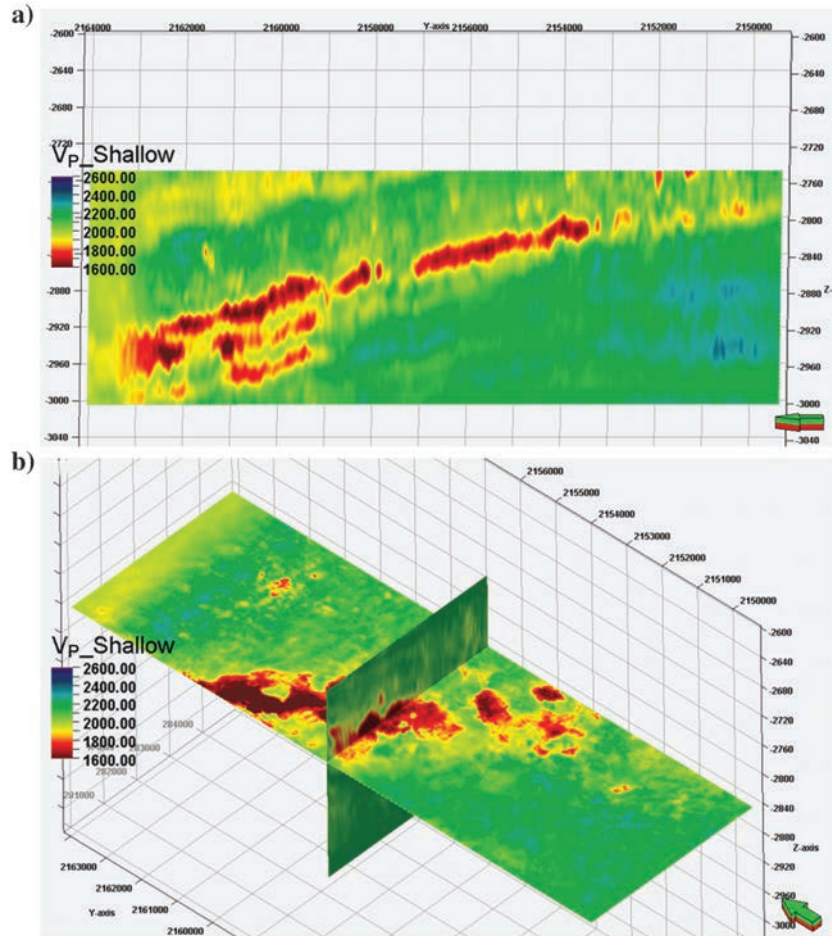

Figure 9. Poststack inversion result using (a) ray tomography velocity model as LFM, (b) well velocity as LFM, and (c) final FWI velocity as LFM (data processed by ION in partnership with Schlumberger, who holds the data licensing rights).
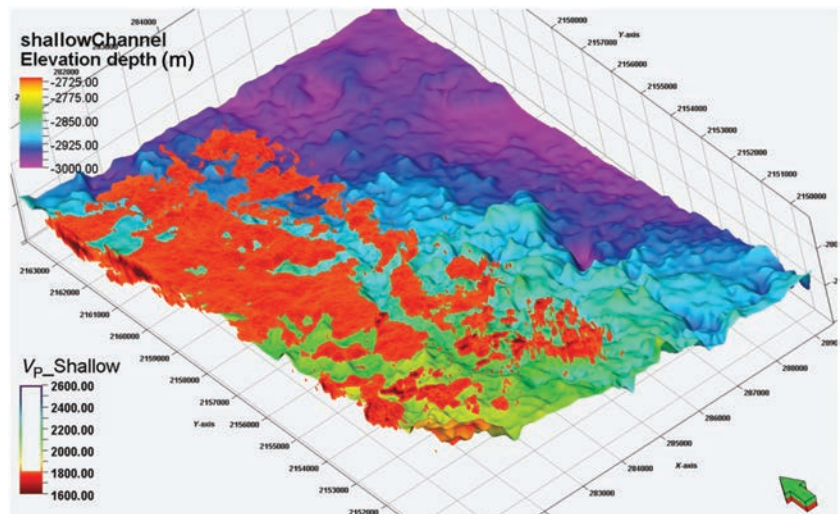
the velocity sections of Figure 3. We note that the velocities at this well are in error up to a depth of 2600 m because these velocities are too fast for generating a good image, but at higher depths, the final FWI inverted velocity resulted in a high correlation at the two wells

(only one is shown for brevity). The RTM image overlying the final velocity shown in Figure 3d highlights the degree of detail incorporated into the velocity model by the three combined approaches. The modeled synthetic data for the final FWI model shown in Figure 2c and 2f predict all events with a high accuracy in the displayed time window. The staging in the model-building flow, from low to high frequencies and shallow to deep, reduces potential cycle skipping problems while matching the waveforms.

Figure 4a and 4b shows Kirchhoff prestack depth-migrated stack and gathers produced with the reflection tomography model of Figure 3a, and Figure 4c and 4d shows stack and gathers for the final inverted velocity model in Figure 3c for a different inline than the one displayed in Figures 2 and 3. The improvement in stack quality is relatively small because the tomography model already produces relatively flat gathers. Migration with the final FWI model produces a slight shift of reflectors laterally and in depth for the stack image. Gathers show an improved flatness resulting in a relatively small enhancement in the lateral continuity of events. Figure 5a–5c shows a horizontal slice at a depth of 2860 m extracted from the ray-based reflection tomography velocity model, the final FWI + RWI inverted velocity model, and the final stack image, respectively. The observed details in the final FWI velocity are mainly the product of the first FWI stage, which highlights some low-velocity areas not observed in the tomography model and a clear fault passing through the flank of the anticline also observed in the final stacked image.

Figure 10. Shallow stacked sand in (a) the inline direction and (b) 3D views (data processed by ION in partnership with Schlumberger, who holds the data licensing rights).

Figure 11. Shallow stacked sand — 3D top view (data processed by ION in partnership with Schlumberger, who holds the data licensing rights).

Figure 6a–6c shows a deeper slice (4620 m) through the tomography velocity model, the final FWI + RWI velocity model, and the final image, respectively. Model updates with the RWI method resulted in velocity perturbations delineating sand channels and faults. Figure 7 shows a comparison of the well sonic velocities with the different stages of velocity model-building results. The agreement observed between the well sonic velocity and the final estimated velocity motivates the application of a conventional acoustic impedance inversion described in the following section for further enhancing this result. Two short videos illustrate the evolution of the process: Supplementary information that can be accessed through the following link: S1.mpg shows the modeled data for a common channel, 4000 m offset in average. These modeled data are represented by the green wiggles overlaid on the field data represented by the reference static black wiggles. The modeled data are modeled making use of the inverted velocity obtained after each consecutive iteration of FWI or RWI. Supplementary information that can be accessed through the following link: S2.mpg shows the corresponding velocity for an inline section, starting from the initial ray-based tomography velocity up to the final RWI velocity (Figure 8).

Poststack inversion results

Making use of a standard poststack inversion method (Russell and Hampson, 1991), we performed three different poststack velocity inversions. The first one is using the ray-based tomography velocity as an LFM, the second one is using the velocity from one of the wells extrapolated with the structural interpretation from the stack, and the third one is using the final FWI + RWI velocity as an LFM. An underlying assumption is the Gardner relationship between density and velocity in the process. These results are displayed, respectively, in Figure 9a–9c for the same inline as displayed in Figures 2 and 3. The LFM made from the ray-based tomography velocity (Figure 9a) contains a smooth velocity trend; thus, it does not contain enough bandwidth overlap with the bandwidth from the stack to produce an enhanced
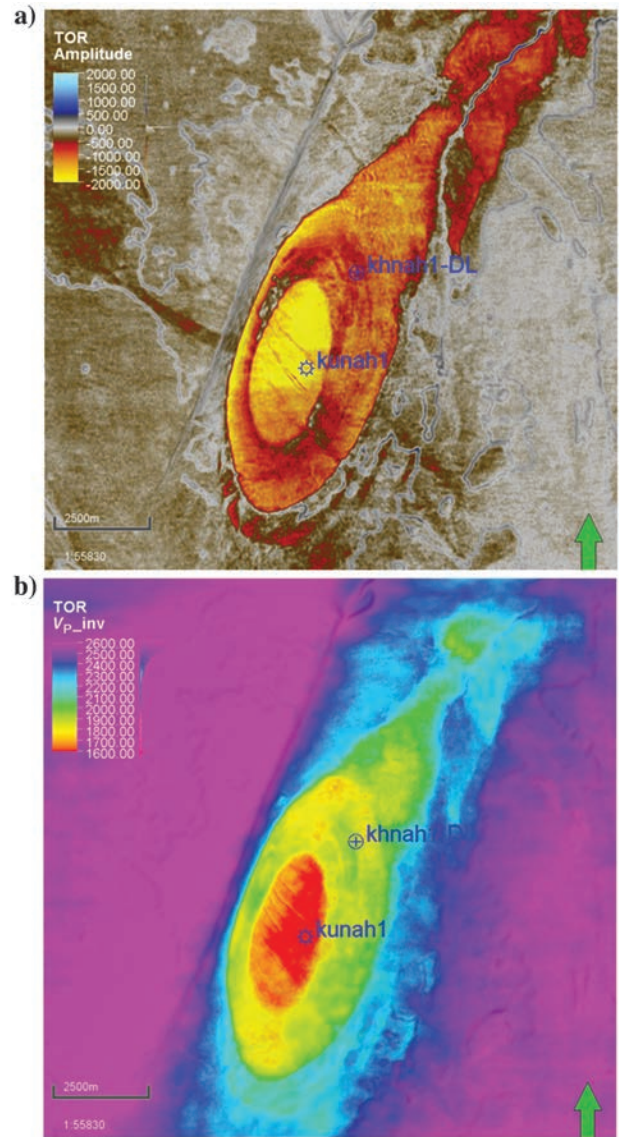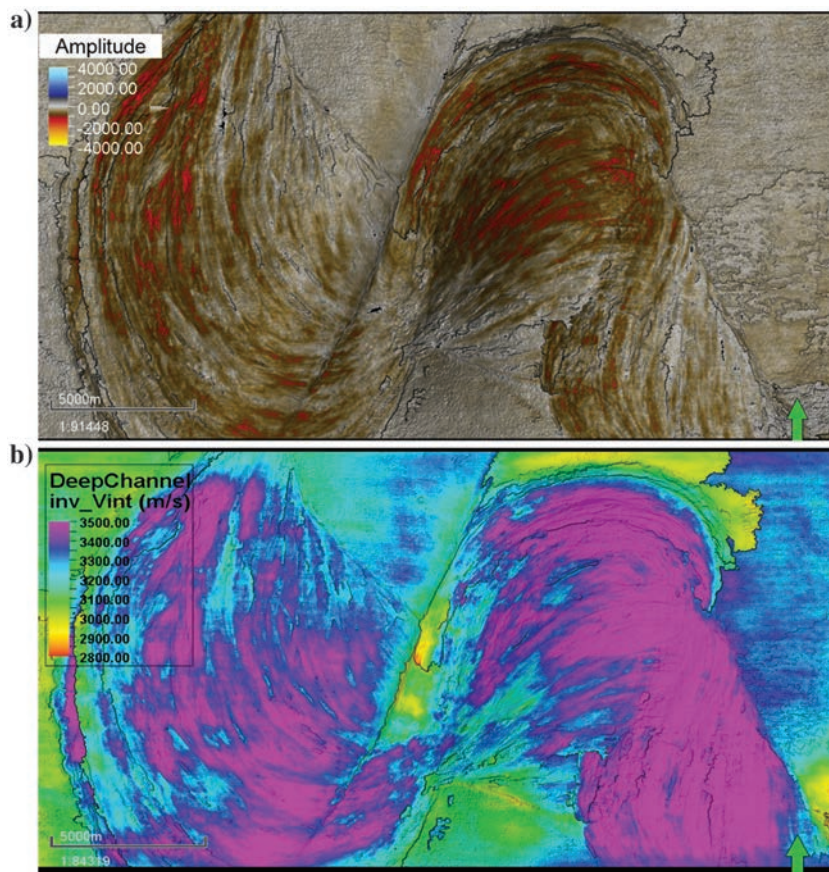

Figure 13. (a) Amplitude extraction top of reservoir and (b) poststack amplitude inversion derived velocity at top of reservoir (data processed by ION in partnership with Schlumberger, who holds the data licensing rights).
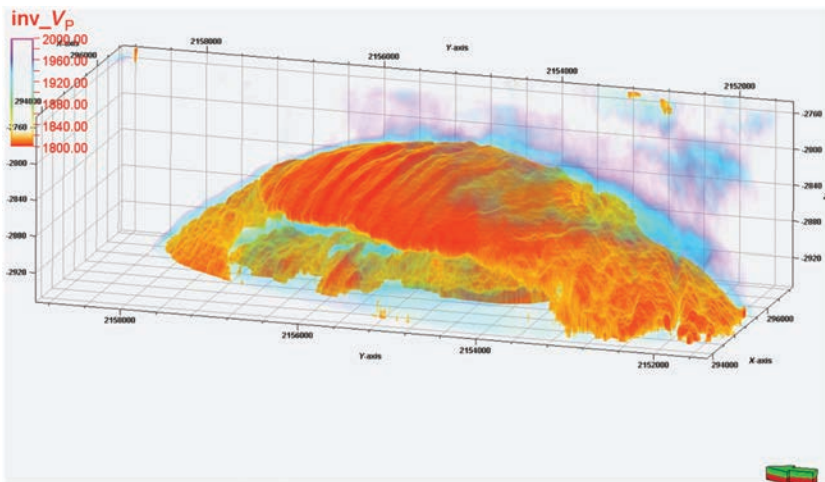
Figure 12. Geobody extracted from low-velocity anomaly defines the reservoir (data processed by ION in partnership with Schlumberger, who holds the data licensing rights).
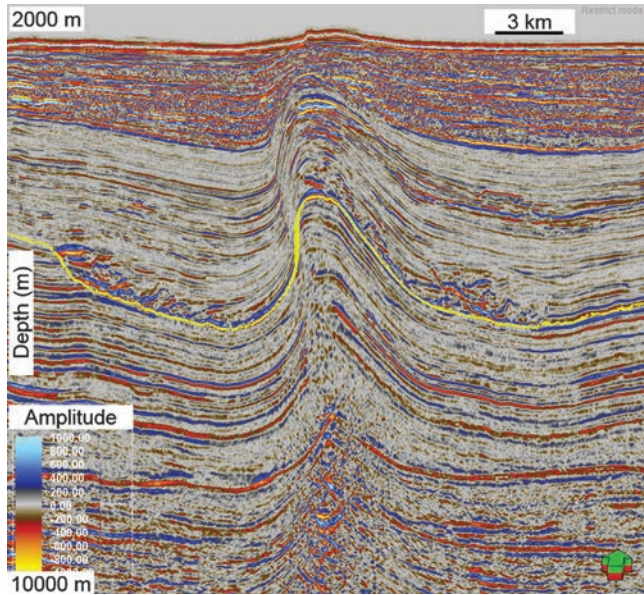
Figure 14. The 60 Hz RTM stack showing yellow horizon used for amplitude and velocity attribute extraction (data processed by ION in partnership with Schlumberger, who holds data licensing rights).

Figure 15. (a) Amplitude extraction from 60 Hz RTM stack along yellow horizon at base of channel complex and (b) poststack amplitude inversion derived velocity extracted along yellow horizon (data processed by ION in partnership with Schlumberger, who holds the data licensing rights).

poststack inversion result. The traditional approach that uses well velocities as an LFM with a structural framework (Figure 9b) produces what is likely to be a biased velocity away from the well, extending relatively low reservoir velocities at the well into nonreservoir formations. Within the reservoir, the structure seems to possess significant heterogeneity, which makes the extrapolation of well velocity challenging. Furthermore, as discussed in the previous section, the shallow velocities from the well are too fast based on imaging results with the seismic well tie also indicating that most likely the overburden velocities at the well are in error. The final FWI + RWI model-building flow here applied bypasses some of the pitfalls of the classical quantitative seismic inversion requiring in some cases detailed structural and stratigraphic interpretation. The poststack velocity inversion result using the final FWI + RWI velocity as LFM (Figure 9c) shows a distinct anomaly conforming to the top of an enclosed structure high also observed in the stack image and a flat base. This structure has been drilled and proven to be a gas/wet gas reservoir. The poststack amplitude inversion further sharpened the resolution of the final velocity field.

Figure 10a and 10b shows 2D and 3D views, respectively, corresponding to a shallow region (2750–2900 m) of relatively low velocities from the final poststack velocity inversion result of Figure 9c, highlighting the presence of sand bodies and what appears to be three episodes of sand distribution. Figure 11 shows a top view of these bodies with an enhanced color palette and a high velocity transparency. Low-velocity geobodies below the mudline are clearly notable. A higher velocity channel can be seen meandering through the sand bodies. These bodies are not observed on the east side of the study area. Figures 12 and 13 display detail views of the top of the reservoir using transparency and an enhanced velocity color palette (Figure 12), extracted amplitudes form the final image (Figure 13a), and final FWI velocities after poststack inversion (Figure 13b) in map view displays. The lower limit of the reservoir can be interpreted clearly (Figure 12) and the amplitude extraction on the reservoir top structure maps (Figure 13), which show the discovery well drilled near the crest and a dry delineation well drilled down dip below the gas-water contact. The geobody outlined by the low-velocity anomaly defines the geologic extent of the gas reservoir. Using a rock-physics model relating velocity to gas saturation and porosity, the reservoir properties could be estimated via a Bayesian inversion for quantitative analysis.

In the deeper section, a velocity inversion reveals potential channels (3800–5000 m), shown in the highlighted horizon overlaying the stack section in Figure 14. Figure 15a and 15b shows, respectively, autotracked seismic amplitudes and velocities from the final poststack inverted result along the interpreted base-of-channel horizon on both sides of the anticline structure cut by a reverse fault. The displays show that the channels likely belong to a single channel with an approximate maximum width of 4200 m in this study area. We interpret this meandering channel as being uplifted and then cut by the fault system. Based on the rock physics knowledge of the area, at shallow depths, the sand velocity is slower than that of shale formations; at a higher depth, the sand velocity becomes faster than that of the surrounding shale most likely due to compaction. Therefore, we interpret the channel to be sand filled, with the differential velocity in the channel reflecting the burial depth and history of the sand formation. Figure 16a and 16b displays the same attribute map in a 3D structural framework for the final FWI velocity and its corresponding poststack inversion result. The waveform inversion result provides a meaningful structural and stratigraphic detail that is enhanced by the poststack inversion process, in this case further highlighting the presence of the sand bodies.

Conclusion

We presented a model-building flow combining reflection tomography, diving wave FWI, RWI, and standard poststack inversion for building an interpretable velocity property volume. The inversion is acoustic and uses diving waves and reflections resulting in a high-resolution velocity model for imaging. The derived velocities are in relatively good agreement with velocities from two wells in the area of investigation. The inverted velocity model can be used to delineate geologic features such faults and sand channels and as a product for other applications such as amplitude inversion and direct reservoir prospecting and delineation. Using the final FWI + RWI velocity as the background model, the flow incorporates geology variations contained in the seismic data, and potentially bypasses a heavily involved geologic interpretation. This approach might overcome potential pitfalls due to lack of enough well velocity constrains for background velocity model building in a classic amplitude-based inversion process. We have used this product for delineating a gas reservoir and a deep meandering channel. Integrating LFM from the final FWI + RWI model and amplitude inversion using high-frequency content in the migrated seismic data potentially produces less biased rock properties for reservoir characterization. The suggested workflow is approximately one to two orders of magnitude more expensive computationally than a more standard workflow that is based on tomography updates only, and it is mostly automatic. It also avoids a more intensive FWI process that considers elastic propagation.
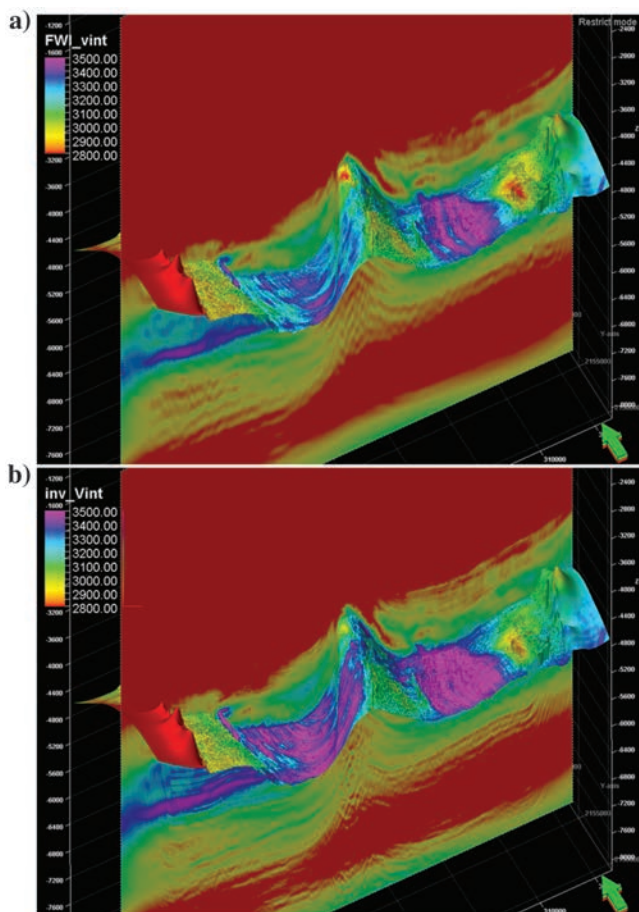
Data and materials availability

Data associated with this research are confidential and cannot be released.

Figure 16. (a) The 3D view of final FWI velocity extraction along yellow horizon reveals a meandering sand-filled channel highlighted by fast velocity and (b) 3D view poststack amplitude inversion derived velocity extraction along yellow horizon reveals more details of a meandering sand-filled channel highlighted by fast velocity (data processed by ION in partnership with Schlumberger, who holds the data licensing rights).

References

Brossier, R., S. Operto, and J. Virieux, 2013, Toward data-domain waveform inversion of reflected waves: 83rd Annual International Meeting, SEG, Expanded Abstracts, 892–897, doi: 10.1190/segam2013-0897.1.

Chang, W.-F., and G. A. McMechan, 1994, 3-D elastic prestack, reverse-time depth migration: Geophysics, **59**, no. 4, 599–607, doi: 10.1190/1.1443620.

Chen, J., D. Sixta, G. Raney, V. Mount, E. Riddle, A. Nicholson, H. Ma, H. Ji, and C. Peng, 2018, Improved sub-salt imaging from reflection full waveform inversion guided salt scenario interpretation: A case history from deep water Gulf of Mexico: 88th Annual International Meeting, SEG, Expanded Abstracts, 3773–3777, doi: 10.1190/segam2018-2996573.1.

Huang, Y., B. Bai, H. Quan, T. Huang, S. Xu, and Y. Zhang, 2011, Application of RTM 3D angle gathers to wide-azimuth data subsalt imaging: Geophysics, **76**, no. 5, WB175–WB182, doi: 10.1190/geo2010-0396.1.

Liu, Y., J. Yang, B. Chi, and L. Dong, 2015, An improved scattering-integral approach for frequency-domain full waveform inversion: Geophysical Journal International, **202**, 1827–1842, doi: 10.1093/gji/ggv254.

Lu, R., S. Lazaratos, K. Wang, Y. H. Cha, I. Chikichev, and R. Prosser, 2013, High-resolution elastic FWI for reservoir characterization: 75th Annual International Conference and Exhibition, EAGE, Extended Abstracts, doi: 10.3997/2214-4609.20130113.

Peng, C., M. Wang, N. Chazalnoel, and A. Gomes, 2018, Subsalt improvement possibilities through a combination of FWI and reflection FWI: The Leading Edge, **37**, 52–57, doi: 10.1190/tle37010052.1.

Routh, P., R. Neelamani, R. Lu, S. Lazaratos, H. Braaksma, S. Hughes, R. Saltzer, J. Stewart, K. Naidu, H. Averill, V. Gottumukkula, P. Homonko, J. Reilly, and D. Leslie, 2017, Impact of high-resolution FWI in the Western Black Sea: Revealing overburden and reservoir complexity: The Leading Edge, **36**, 60–66, doi: 10.1190/tle36010060.1.

Russell, B., and D. Hampson, 1991, A comparison of post-stack seismic inversion methods: 61st Annual International Meeting, SEG, Expanded Abstracts, 876–878, doi: 10.1190/1.1888870.

Sams, M., and D. Carter, 2017, Stuck between a rock and a reflection: A tutorial on low-frequency models for seismic inversion: Interpretation, **5**, no. 2, B17–B27, doi: 10.1190/INT-2016-0150.1.

Sirgue, L., and R. Pratt, 2004, Efficient waveform inversion and imaging: A strategy for selecting temporal frequencies: Geophysics, **69**, 231–248, doi: 10.1190/1.1649391.

Tarantola, A., 1984, Inversion of seismic reflection data in the acoustic approximation: Geophysics, **49**, 1259–1266, doi: 10.1190/1.1441754.

Van Leeuwen, T., and F. Hermann, 2013, Mitigating local minima in full-waveform inversion by expanding the search space: Geophysical Journal International, **195**, 661–667, doi: 10.1093/gji/ggt258.

Vigh, D., K. Jiao, X. Cheng, D. Sun, and W. Lewis, 2016, Earth-model building from shallow to deep with full-waveform inversion: The Leading Edge, **35**, 1025–1030, doi: 10.1190/tle35121025.1.

Virieux, J., and S. Operto, 2009, An overview of full-waveform inversion in exploration geophysics: Geophysics, **74**, no. 6, WCC1–WCC26, doi: 10.1190/1.3238367.

Wang, C., D. Yingst, J. Brittan, P. Farmer, and J. Leveille, 2014, Fast multi-parameter anisotropic full waveform inversion with irregular shot sampling: 84th Annual International Meeting, SEG, Expanded Abstracts, 1147–1150, doi: 10.1190/segam2014-0234.1.

Wang, C., D. Yingst, P. Farmer, I. Jones, G. Martin, and J. Leveille, 2017, Reconstructed waveform inversion with the extended source: 87th Annual International Meeting, SEG, Expanded Abstracts, 1449–1453, doi: 10.1190/segam2017-17736054.1.

Yang, J., Y. Liu, and L. Dong, 2016, Simultaneous estimation of velocity and density in acoustic multi-parameter full-waveform inversion using an improved scattering-integral approach: Geophysics, **81**, no. 6, R399–R415, doi: 10.1190/geo2015-0707.1.

Zhang, Z., J. Mei, F. Lin, R. Huang, and P. Wang, 2018, Correcting for salt misinterpretation with full-waveform inversion: 88th Annual International Meeting, SEG, Expanded Abstracts, 1143–1147, doi: 10.1190/segam2018-2997711.1.

Yannick Cobo received an engineer degree (1990) from Ecole Nationale Superieure de Geologie and a M.S. in mineral and energetic raw materials from Institut National Polytechnique de Lorraine, France. He has 25 year experience in seismic data processing and imaging for the oil & gas industry. He is currently a geophysical advisor at ION Geophysical. His technical interests include seismic imaging and modeling, and the use of FWI inversion to derive earth models. He is a member of the professional societies SEG and EAGE.

Carlos Calderón-Macías has a bachelor's degree in Geophysical Engineering from the National Autonomous University of Mexico and a Ph.D. from the University of Texas at Austin. He then worked at Mobil Technology and joined the Institute of Mexican Petroleum afterwards as a researcher. He is currently a senior advisor at ION Geophysical. His main interests are in seismic wave propagation topics such as multicomponent seismology, model estimation, signal processing and near surface geophysics. He is a member of SEG and EAGE.

Dr. Shihong Chi is a Senior Geophysical Advisor at E&P Advisors Group within ION Geophysical with over 13 years of industry experiences. His interest is primarily in integration of multi-disciplinary data for reservoir characterization. He conducted his Post-Doctoral research in Geophysics at Massachusetts Institute of Technology from 2004 to 2006. He obtained his Master in 1999 and

Ph.D. in Petroleum Engineering, at the University of Texas at Austin in 2003. He joined ConocoPhillips working on petrophysics and rock physics in 2006. At Marathon Oil, he enjoyed working on seismic reservoir characterization of deep water and unconventional reservoirs. At BHP Billiton, his work was focused on rock physics, seismic attributes and facies classification integrating well and seismic inversion results for unconventional and conventional reservoirs. At ION, his effort has been to integrate seismic inversion and well data to provide high resolution reservoir model for optimization of unconventional reservoir development. He has been engaged in high end sonic shear, and VTI and HTI anisotropy development processing, calibration and QC over the past 20 years. His expertise is in the following areas: Rock physics for conventional and unconventional reservoirs; advanced sonic data processing and applications for rock physics and anisotropy interpretation; Seismic AVO inversion and quantitative interpretation; Seismic attribute analyses; Reservoir characterization; Multidisciplinary data integration.